



ELSEVIER

Contents lists available at ScienceDirect

## Comptes Rendus Biologies

www.sciencedirect.com



Physiology/Physiologie

## Comparative statistical mechanics of myosin molecular motors in rat heart, diaphragm and tracheal smooth muscle

*Mécanique statistique comparative du cœur, du diaphragme et du muscle trachéal de rat*

Yves Lecarpentier<sup>a,\*,b,c</sup>, Victor Claes<sup>d</sup>, Édouard Lecarpentier<sup>c</sup>, François-Xavier Blanc<sup>e</sup>, Thierry Joseph<sup>f</sup>, Bart Geraets<sup>d</sup>, Xénophon Krokidis<sup>a</sup>, Jean-Louis Hébert<sup>a,b</sup>

<sup>a</sup> Service de physiologie, hôpital de Bicêtre, Assistance publique–Hôpitaux de Paris, 94275 Le Kremlin-Bicêtre, France

<sup>b</sup> Université Paris-11, 94275 Le Kremlin-Bicêtre, France

<sup>c</sup> Centre de recherche clinique, CHR de Meaux, 77100 Meaux, France

<sup>d</sup> Department of Pharmaceutical Sciences, University of Antwerp, Wilrijk, Belgium

<sup>e</sup> Unité de pneumologie, service de médecine interne, hôpital de Bicêtre, Assistance publique–Hôpitaux de Paris, 94275 Le Kremlin-Bicêtre, France

<sup>f</sup> Service de cardiologie, hôpital Laennec, centre hospitalier intercommunal de Cornouaille, 29000 Quimper, France

## ARTICLE INFO

## Article history:

Received 25 September 2010

Accepted after revision 2 August 2011

## Keywords:

Statistical mechanics

Entropy production rate

Heart

Diaphragm

Tracheal smooth muscle

## ABSTRACT

**Purpose.** – Statistical mechanics establishes a link between microscopic properties of matter and its bulk properties. A. Huxley's equations (1957) [1] provide the necessary phenomenological formalism to use statistical mechanics.

**Methods.** – We compared statistical mechanics in rat diaphragm in tetanus (tet;  $n = 10$ ) and twitch (tw;  $n = 12$ ) modes, in heart in twitch mode ( $n = 20$ ), and in tracheal smooth muscle in tetanus mode (TSM;  $n = 10$ ). This powerful tool makes it possible to determine: (i) statistical entropy ( $S$ ) which is related to the dispersal of energy and represents a measure of the degree of disorder in muscular system; (ii) thermodynamic force  $A/T$  (chemical affinity  $A$  and temperature  $T$ ); (iii) thermodynamic flow ( $v$ ); (iv) entropy production rate ( $A/T \times v$ ), which quantifies irreversible chemical processes generated by myosin crossbridge (CB) molecular motors.

**Results.** – All muscles studied operated near equilibrium, i.e.,  $A \ll 2500$  J/mol and in a stationary linear regime, i.e.,  $A/T$  varied linearly with  $v$ . The heart operated farther from equilibrium than both diaphragm (tet and tw) and TSM, as attested by its high entropy production rate.  $S$  was of the same order of magnitude in heart and TSM but lower in diaphragm (tet and tw).

**Conclusion.** – CB kinetics derived from A. Huxley's equations conferred a characteristic profile in terms of statistical mechanics on each muscle type. All studied muscles differed in terms of statistical entropy, chemical affinity, and entropy production rate. Stimulation mode (tet and tw) modulated CB kinetics and statistical mechanics. All muscle types operated near equilibrium and in a stationary linear regime.

© 2011 Académie des sciences. Published by Elsevier Masson SAS. All rights reserved.

\* Corresponding author.

E-mail address: yves.lecarpentier@bct.aphp.fr (Y. Lecarpentier).

## R É S U M É

**Mots clés :**

Mécanique statistique  
 Production d'entropie  
 Cœur  
 Diaphragme  
 Muscle lisse trachéal

**Objectif.** – La mécanique statistique établit un lien entre les propriétés microscopiques et macroscopiques de la matière. Les équations d'A. Huxley (1957) [1] fournissent le formalisme phénoménologique permettant d'appliquer la mécanique statistique aux systèmes musculaires.

**Méthodes.** – Nous avons comparé des résultats de mécanique statistique obtenus dans le diaphragme en mode « tétanique » ( $n = 10$ ) et en mode « twitch » ( $n = 12$ ), dans le cœur en mode « twitch » ( $n = 20$ ) et dans le muscle trachéal en mode « tétanique » ( $n = 12$ ) chez le rat, en déterminant l'entropie statistique ( $S$ ), la force thermodynamique ( $A/T$ ;  $A$  étant l'affinité et  $T$  la température absolue), le flux thermodynamique ( $v$ ) et la vitesse de production d'entropie ( $A/T \times v$ ).

**Résultats.** – Tous les muscles dans cette étude opèrent de façon proche de l'équilibre ( $A \ll 2500 \text{ J/mol}$ ) et en régime linéaire stationnaire ( $A/T$  proportionnel à  $v$ ). Le cœur fonctionne plus loin de l'équilibre que les autres muscles comme en atteste la grande vitesse de production d'entropie de ce muscle par rapport aux autres.  $S$  est du même ordre de grandeur dans le cœur et le muscle trachéal, mais est plus basse dans le diaphragme en twitch et en tétanus que dans le cœur et le muscle trachéal.

**Conclusion.** – Les cinétiques des ponts actine-myosine calculées à partir des équations d'A. Huxley confèrent à chaque type de muscle un profil spécifique en matière de mécanique statistique. Le mode de stimulation (tétanique ou twitch) influence les cinétiques des ponts actine-myosine et leur comportement en termes de mécanique statistique. Tous les muscles étudiés demeurent proches de l'équilibre et en régime stationnaire.

© 2011 Académie des sciences. Publié par Elsevier Masson SAS. Tous droits réservés.

## 1. Introduction

In muscular tissues, the huge number of myosin II heads or crossbridges (CBs) involved in contractile processes provides the necessary ground for applying statistical mechanics. This field of physical sciences represents a powerful tool for establishing links between the microscopic and macroscopic thermodynamic properties of physical and biological systems [2]. Statistical mechanics makes it possible to determine: (i) the statistical entropy of a given system which represents a measure of the degree of disorder; (ii) entropy production rate, quantifying irreversible chemical processes [3]; (iii) other macroscopic thermodynamic properties. For statistical mechanics to be applied in living muscles, a phenomenological description of the behavior of CB molecular motors is needed, and this is provided by A. Huxley's equations [1]. These equations establish a relationship between CB kinetics and the mechanics of the whole muscle. Moreover, they make it possible to determine the probability of several steps of the CB actomyosin cycle [4]. This represents the cornerstone of the process of using statistical mechanics as a tool for mathematical treatment of A. Huxley's phenomenological formalism.

Living organisms are open systems and consequently are not in thermodynamic equilibrium. They are maintained in a non-equilibrium state by a flow of energy and matter. They may operate either near or far from thermodynamic equilibrium [3]. Numerous cellular systems have been shown to behave in a near-equilibrium state and in linear stationary regime [5]. Other living systems operate far from equilibrium [6]. Slow (Soleus) and fast (EDL) skeletal muscles [7] and diaphragm muscle [8] contracting under tetanic conditions have recently

been reported to work in a stationary linear regime where thermodynamic force linearly varies with thermodynamic flow [3]. However, skeletal muscles under twitch conditions, heart muscle and tracheal smooth muscle have not been investigated in terms of thermodynamic force and flow. The aim of the present study was to apply statistical mechanics to both striated and smooth muscles, i.e., in diaphragm (in twitch and tetanus), heart and tracheal smooth muscle (TSM). Thermodynamic properties such as statistical entropy, internal energy, chemical affinity, thermodynamic force, thermodynamic flow and entropy production rate were determined and characterized each type of muscle studied. We showed that these muscles behaved in a near equilibrium manner and in a stationary linear regime.

## 2. Materials and methods

### 2.1. Animals

All procedures conformed to the Guide for Care and Use of Laboratory Animals and were approved by the local committee of our institution. Animals were 3-month-old male rats and were housed under controlled temperature (20–22 °C) and lighting (12-h light-dark cycle), with free access to food and water.

### 2.2. Experimental setup

Mechanical experiments were conducted on diaphragm and heart muscles, and TSM from Wistar rats. Animals were sacrificed after anaesthesia with intraperitoneal injection of sodium pentobarbital (60 mg/kg). Each muscle strip was rapidly mounted in a chamber containing a

Krebs-Henseleit solution (in mM): 118 NaCl, 4.7 KCl, 1.2 MgSO<sub>4</sub>·7H<sub>2</sub>O, 1.1 KH<sub>2</sub>PO<sub>4</sub>, 24 NaHCO<sub>3</sub>, 2.5 CaCl<sub>2</sub>·6H<sub>2</sub>O and 4.5 glucose and bubbled with 95% O<sub>2</sub>–5% CO<sub>2</sub> and maintained at pH 7.4 and 26 °C (diaphragm strips; *n* = 12 in twitch [tw] and *n* = 10 in tetanus [tet]) (two diaphragm strips in tet were unstable and were discarded), 29 °C (cardiac papillary muscles; *n* = 20) and 37 °C (TSM; *n* = 10). For each muscle type, the chosen temperature induced stability and the best mechanical performance. Muscles were electrically stimulated by means of two platinum electrodes delivering either twitch or tetanic stimulation. In cardiac muscle: twitch stimulation (electrical stimulus: 5 ms duration; stimulation frequency: 10/min). In diaphragm: twitch stimulation (electrical stimulus: 1 ms duration; stimulation frequency: 10/min), and tetanic stimulation (electrical stimulus: 1 ms duration; stimulation frequency: 50 Hz; train duration: 250 ms; train frequency: 6/min). In TSM: tetanic stimulation (electrical stimulus: 5 ms duration; stimulation frequency: 50 Hz; train duration: 12 s; train frequency: every 3 min). The electromagnetic lever system has been described earlier [9].

### 2.3. Muscle and crossbridge mechanics

Maximum unloaded shortening velocity ( $V_{max}$ , in  $Lo \cdot s^{-1}$ ) was measured by means of the zero-load technique. Maximum isometric force ( $F_0$ ) was measured from the isometric contraction at  $L_0$ , the initial length corresponding to the apex of the active tension-initial length relationship. Maximum isometric tension ( $P_0$  in  $mN \cdot mm^{-2}$ ) (Fig. 1) was obtained by normalizing  $F_0$  per muscle cross-sectional area. Muscle mechanical

parameters and those determined from Hill's equation [10] have previously been described [11].  $V_{max}$  was determined by means of the zero-load clamp technique with a damping which induced only one oscillation just after the clamp on the phase-plane velocity-length relationship. Seven to ten isotonic load levels ( $P$ ) were performed. The tension versus time curves and length versus time curves were represented at various load levels for each muscle type in Fig. 1. The tension-velocity ( $P$ - $V$ ) relationship was fitted according to Hill's equation  $(P + a)(V + b) = (P_0 + a)b$ , where  $-a$  and  $-b$  are the asymptotes of the hyperbola as determined by multilinear regression. For each muscle, the  $P$ - $V$  relationship was accurately fitted by a hyperbola. Values of the  $r$  coefficient of correlation were  $0.98 \pm 0.01$  in diaphragm (tet),  $0.90 \pm 0.07$  in diaphragm (tw),  $0.86 \pm 0.08$  in heart and  $0.98 \pm 0.01$  in TSM (means  $\pm$  standard deviations (SD)). These values did not differ between heart and diaphragm (tw) and between diaphragm (tet) and TSM and were higher in diaphragm (tet) and TSM than in diaphragm (tw) and heart ( $P < 0.05$ ). The  $G$  curvature of Hill's equation was equal to  $P_0/a = V_{max}/b$ , [10,12].

A. Huxley's equations [1] were used to calculate the constants of CB attachment ( $f_1$  in  $s^{-1}$ ) and detachment ( $g_1$  and  $g_2$  in  $s^{-1}$ ), maximum turnover rate of myosin ATPase under isometric conditions ( $k_{cat}$  in  $s^{-1}$ ), elementary force per single CB ( $\pi$  in pN), number of active CBs per cross-sectional area ( $N$ ), maximum efficiency, mean CB velocity, frictional drag force (FDF), and time stroke ( $t_s$ ) [9] (Fig. 2D). A. Huxley's equations can be applied to striated muscles in steady state isotonic tetanus. They can also be used in smooth muscles in tetanic conditions as proposed by

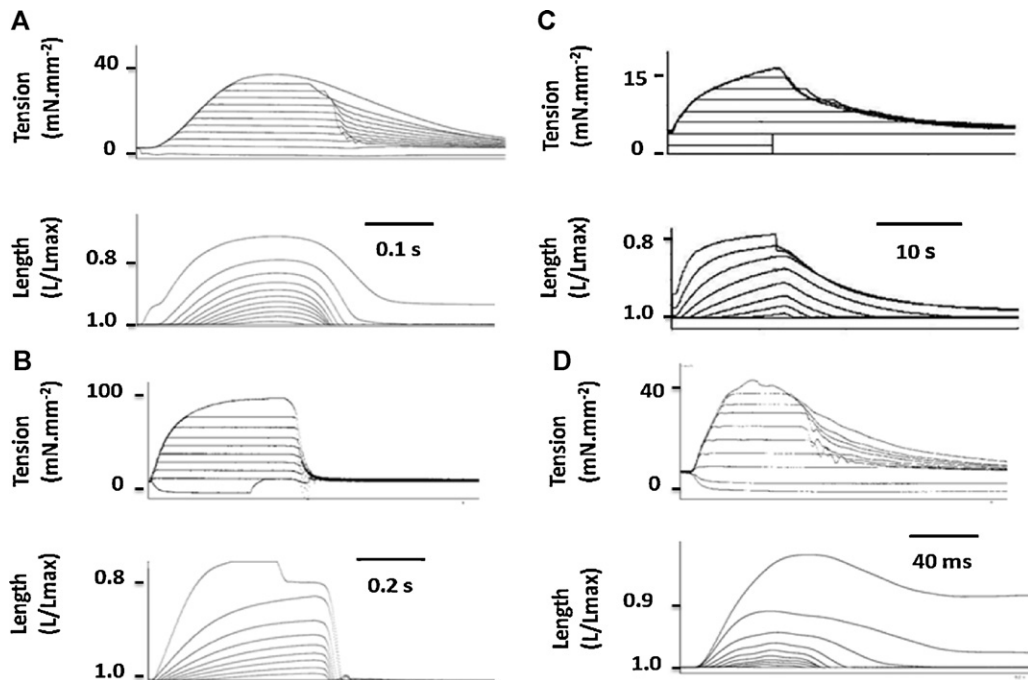
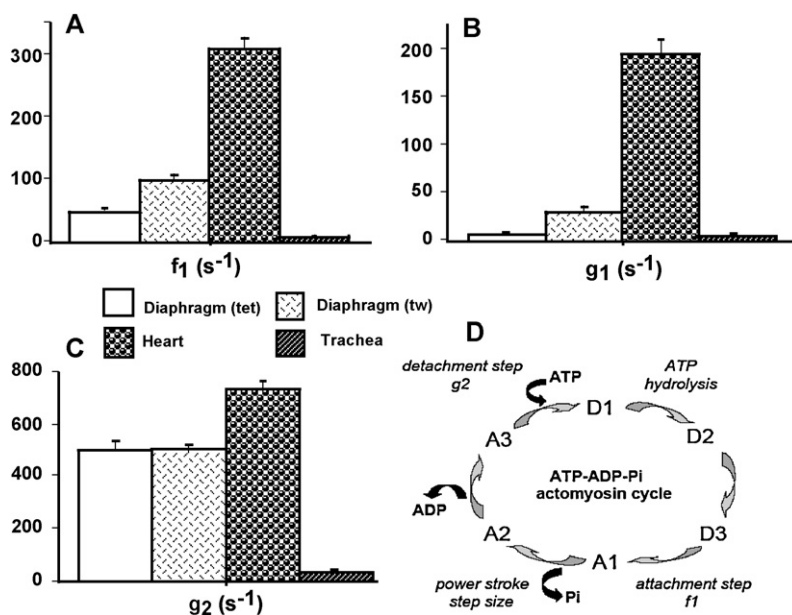


Fig. 1. Heart (A); Diaphragm (tet) (B); TSM (C); Diaphragm (tw) (D). In each panel, tension versus time curves (upper traces) and length versus time curves (lower traces) were represented at various load levels.



**Fig. 2.** CB kinetic properties and CB cycle. Attachment constant  $f_1$  (A); detachment constants  $g_1$  and  $g_2$  (B and C, respectively); CB cycle (D): The ATP-ADP-Pi-actomyosin CB cycle. The CB cycle was subdivided into six different conformational states, with three detached states (D1, D2, and D3) and three attached states (A1, A2, and A3). Transition A3→D1 was the ATP binding step; CB detachment occurred when ATP bound to the actin (A)-myosin (M) complex (AM) and the rate constant for detachment was  $g_2$ ;  $AM + ATP \rightarrow A + M-ATP$ . Transition D1→D2 was the ATP hydrolysis;  $M-ATP \rightarrow M-ADP-Pi$ . Transition D2→D3 was  $M-ADP-Pi \rightarrow M^*-ADP-Pi$ . Transition D3→A1 was the weakly bound attachment state: the myosin head ( $M^*-ADP-Pi$ ) weakly bound to A and the rate constant for attachment was  $f_1$ ;  $M^*-ADP-Pi + A \rightarrow AM-ADP-Pi$ . Transition A1→A2 was the power stroke or strongly bound state which is triggered by Pi release:  $AM-ADP-Pi \rightarrow AM-ADP + Pi$ . Transition A2→A3 was the release of the hydrolysis product ADP:  $AM-ADP \rightarrow AM + ADP$ .

A. Huxley in his princeps study [1,9]. Calculations of  $f_1$ ,  $g_1$ , and  $g_2$  were based on the following equations [8]:

$$G = f_1/g_1 \quad g_1 = (2wb)/(eGh) \quad g_2 = (2Vmax)/h$$

$$k_{cat} = (h/2l) \times [(f_1g_1)/(f_1 + g_1)] \text{ and}$$

$$\pi = (w/l) \times [(f_1)/(f_1 + g_1)]$$

$h$  is the tilt of the myosin head relative to actin; the parameter  $l$  is the distance between successive actin sites with which any myosin site can combine with actin;  $w$  is the maximum mechanical work of a single CB and  $e$  is the free energy required to split one ATP molecule. *In vivo*, the value of  $e = \Delta G^{\circ}_{ATP}$  is nearby  $-60$  kJ/mol, and the value used for  $e$  was  $10^{-19}$  J with  $w = 0.75 e$  [1]. In a whole muscle preparation, we used the  $h = 10$  nm and  $l = 28.6$  nm values which respects A. Huxley's conditions [1]. The estimated value of  $h$  (10 nm) is supported by the three-dimensional head structure of muscle myosin II [13–15]. FDF per CB interaction was  $[(1 - Effmax)/Effmax] \times \pi$ .

#### 2.4. Application of A. Huxley's equations to skeletal and cardiac muscles in twitch

For skeletal muscle and under tetanic electrical stimulation, Hill has shown [10] that the coefficient of shortening heat ("a") and the rate coefficient of total energy liberation during shortening ("b") were similar to the asymptotes ( $-a$  and  $-b$ ) of the characteristic Hill hyperbola  $(P + a)(V + b) = (Po + a)b$ . The rate of total energy liberation has been found to be a linear function of the load, increasing as  $P$  diminishes. This represents the Fenn effect [16]. Importantly, the

theoretical approach of A. Huxley [1] fitted with Hill's results and with the Fenn effect, and the slope of the rate of total energy liberation versus load linear relationship has been found equal to " $-b$ " except at low load [11,12].

The concept of shortening heat has been shown to be applicable to both twitch and tetanus [17]. Thus, in skeletal muscle under twitch conditions, there is a linear negative relationship between the rate of total energy liberation and load level on a large range of load (from 40 to 100% of total load) [12,18]. Mommaerts has unified the concept of Fenn effect [19] which is observed in skeletal (twitch and tetanus) muscle as well as in cardiac muscle [20]. Importantly, as shown by Howard [21], the Fenn effect has been confirmed at the myosin molecular level due to the fact that, at high ATP concentration, the duration of the displacement transient is shorter than that of the force transient, which is precisely what is expected if high load slows down the acto-myosin hydrolysis cycle [22]. Thus, as the Fenn effect: (i) has been described in both twitch skeletal and cardiac muscles; (ii) represents a pivotal property of Huxley's formalism, we proposed to apply this formalism in our study.

#### 2.5. Statistical mechanics

The grand canonical ensemble is a general ensemble for applying statistical mechanics to complex open systems that exchange energy and matter with their surroundings. The formalism used in the present study and which makes it possible to determine the main thermodynamic parameters of the muscle system  $S$  has been previously described

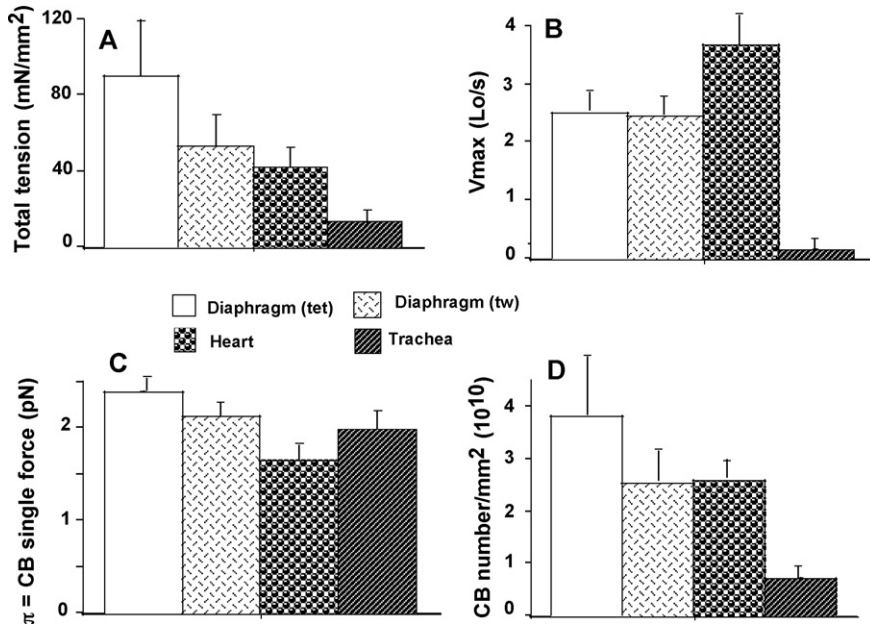


Fig. 3. Total isometric tension (A); Maximum unloaded shortening velocity (Vmax) (B); CB single force (C); CB number/mm<sup>2</sup> (D).

[8], i.e., molar statistical entropy (S), molar internal energy (E), microcanonical (z), canonical (Z) and grand canonical ( $\Xi$ ) partition functions, chemical affinity (A), thermodynamic force (A/T), thermodynamic flow ( $v = kcat/L.mol$ ), and entropy production rate ( $v \times A/T$ ). Thermodynamic flow ( $v$  in  $s^{-1}.L^{-1}.mol$ ) is equal to  $kcat$  (in  $s^{-1}$ ) expressed in  $mol * L^{-1}$ .

2.6. Statistical analysis

Data were expressed as means  $\pm$  standard deviations (SD). After variance analysis, variables of the four groups were compared using the Fisher test. A *P*-value  $< 0.05$  was considered statistically significant. Linear and multilinear regressions were based on the least squares method.

3. Results

3.1. Muscle mechanics

Vmax reached the highest value in heart ( $P < 0.001$  versus the other 3 groups) and the lowest value in TSM

( $P < 0.001$  versus the other 3 groups) (Fig. 3B). Vmax in diaphragm did not differ between twitch and tetanus. Po had the highest value in diaphragm (tet) ( $P < 0.001$  versus the other 3 groups) and had the lowest value in TSM ( $P < 0.001$  versus the other 3 groups) (Fig. 3A). Both the asymptotes  $-a$  and  $-b$  of the P-V hyperbolic relationship were significantly higher in heart than in the other 3 groups ( $P < 0.001$  for each, respectively) (Table 1). The G curvature of the hyperbola was significantly higher in diaphragm (tet) than in the other 3 groups ( $P < 0.001$ ) (Table 1). G was higher in TSM than in heart ( $P < 0.01$ ).

3.2. CB kinetics and mechanics

Attachment ( $f_1$ ) and detachment ( $g_1$ ) constants were dramatically higher in heart than in the other 3 groups ( $P < 0.001$  for each) (Fig. 2A and B). The lowest values of  $f_1$  and  $g_1$  were observed in diaphragm (tet) and TSM, and in both cases there was no difference between the 2 groups. Detachment constant  $g_2$  had the highest value in heart ( $P < 0.001$  versus the other 3 groups) and the lowest value in TSM ( $P < 0.001$  versus the other 3 groups) (Fig. 2C).

Table 1  
Mechanical variables.

	Diaphragm (tet) (n = 10)	Diaphragm (tw) (n = 12)	Heart (n = 20)	TSM (n = 12)
a (mN/mm <sup>2</sup> )	11.9 $\pm$ 1.7	15.1 $\pm$ 1.9	32.8 $\pm$ 2.3	1.9 $\pm$ 0.8
b (Lo/s)	0.32 $\pm$ 0.04	0.64 $\pm$ 0.07	2.04 $\pm$ 0.13	0.06 $\pm$ 0.01
G	8.8 $\pm$ 0.8	4.4 $\pm$ 0.6	1.6 $\pm$ 0.1	2.9 $\pm$ 0.3
z	1.06 $\pm$ 0.01	1.15 $\pm$ 0.03	1.66 $\pm$ 0.04	1.46 $\pm$ 0.04
lnZ* (10 <sup>9</sup> )	2.12 $\pm$ 0.36	3.54 $\pm$ 0.68	13.31 $\pm$ 1.29	2.61 $\pm$ 0.33
ln $\Xi$ * (10 <sup>9</sup> )	1.29 $\pm$ 0.13	0.87 $\pm$ 0.08	9.32 $\pm$ 0.56	1.81 $\pm$ 0.1

-a and -b: asymptotes of the tension-velocity hyperbola. Dimensionless variables: G: curvature of the hyperbola; z: microcanonical partition function; Z: canonical partition function;  $\Xi$ : grand canonical partition function.

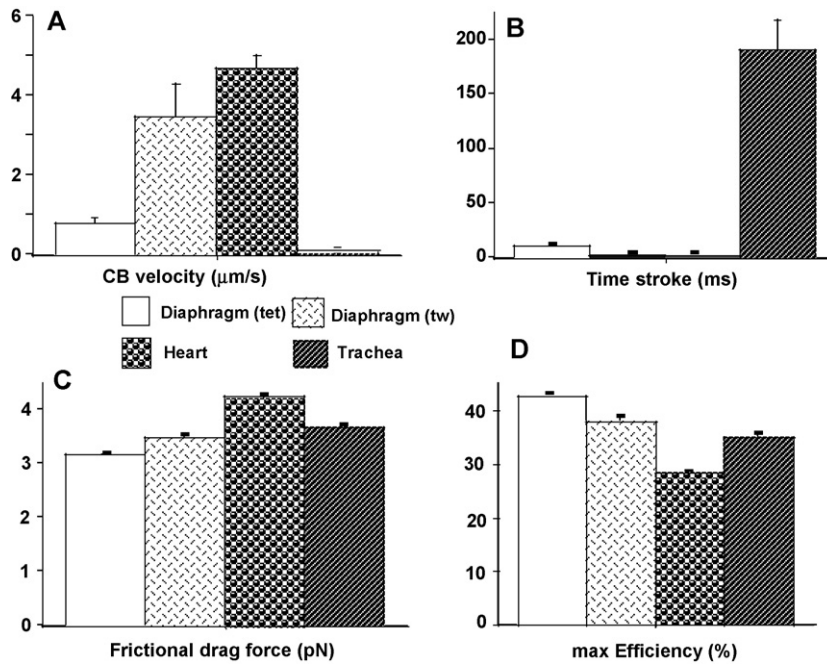


Fig. 4. CB characteristics. CB velocity during power stroke step (A); time stroke (B); frictional drag force (C); max. Efficiency (D).

Detachment constant  $g_2$ , being proportional to  $V_{max}$ , varied as  $V_{max}$ . CB single force ( $\pi$ ) (Fig. 3C) and Effmax (Fig. 4D) reached the highest values in diaphragm (tet) ( $P < 0.001$  versus the other 3 groups, respectively) and the lowest values in heart ( $P < 0.001$  versus the other 3 groups, respectively). Values of  $\pi$  and Effmax in diaphragm (tw) and TSM were intermediate between those of diaphragm (tet) and heart, but were significantly higher in diaphragm (tw) than in TSM. For  $\pi$  and Effmax, all inter-group comparisons gave  $P$  values  $< 0.001$ , except the comparison between diaphragm (tw) and TSM where  $P = 0.07$ . Total number of CB (N) was maximum in diaphragm (tet) and minimum in TSM (for both,  $P < 0.001$  versus the other 3 groups) (Fig. 3D). Frictional drag force (FDF) reached the

highest value in heart and the lowest value in diaphragm (tet) (Fig. 4C). FDF values for diaphragm (tw) and TSM were intermediate between those of heart and diaphragm (tet) but remained significantly lower in diaphragm (tw) than in TSM. For FDF, all inter-group comparisons gave  $P$  values  $< 0.001$ , except for the comparison between diaphragm (tw) and TSM, where  $P = 0.22$ . Mean CB velocity during the stroke step ( $v_0$ ) varied in an opposite manner to that of time stroke  $t_s$  (Fig. 4A and B). The lowest  $v_0$  value was observed in TSM ( $P < 0.001$  versus the other 3 groups, respectively). The highest value of  $t_s$  was observed in TSM ( $P < 0.001$  versus the other 3 groups, respectively). Probabilities of the 6 steps of the CB cycle are presented in Table 2. PD3 had the highest probability in all groups,

Table 2  
Probabilities of the steps of the CB cycle.

	Diaphragm (tet) ( $n = 10$ )	Diaphragm (tw) ( $n = 12$ )	Heart ( $n = 20$ )	TSM ( $n = 12$ )
PD1	$0.0020 \pm 0.0004$	$0.008 \pm 0.002$	$0.028 \pm 0.001$	$0.013 \pm 0.002$
PD2	$0.018 \pm 0.003$	$0.073 \pm 0.015$	$0.248 \pm 0.011$	$0.121 \pm 0.016$
PD3	$0.948 \pm 0.005$	$0.872 \pm 0.020$	$0.610 \pm 0.014$	$0.688 \pm 0.017$
PA1	$0.019 \pm 0.002$	$0.036 \pm 0.003$	$0.067 \pm 0.001$	$0.046 \pm 0.003$
PA2	$0.013 \pm 0.001$	$0.011 \pm 0.001$	$0.047 \pm 0.003$	$0.132 \pm 0.006$
PA3	$3 \times 10^{-6} \pm 2 \times 10^{-8}$	$3 \times 10^{-6} \pm 7 \times 10^{-8}$	$3 \times 10^{-6} \pm 3 \times 10^{-8}$	$5 \times 10^{-6} \pm 1 \times 10^{-7}$
–PD1 * lnPD1	$0.012 \pm 0.002$	$0.037 \pm 0.006$	$0.099 \pm 0.003$	$0.057 \pm 0.006$
–PD2 * lnPD2	$0.069 \pm 0.010$	$0.175 \pm 0.022$	$0.341 \pm 0.004$	$0.246 \pm 0.018$
–PD3 * lnPD3	$0.050 \pm 0.005$	$0.117 \pm 0.016$	$0.298 \pm 0.007$	$0.255 \pm 0.010$
–PA1 * lnPA1	$0.075 \pm 0.005$	$0.118 \pm 0.008$	$0.180 \pm 0.002$	$0.140 \pm 0.006$
–PA2 * lnPA2	$0.056 \pm 0.002$	$0.051 \pm 0.001$	$0.142 \pm 0.007$	$0.266 \pm 0.006$
–PA3 * lnPA3	$46 \times 10^{-5} \pm 26 \times 10^{-7}$	$4 \times 10^{-5} \pm 8 \times 10^{-7}$	$4 \times 10^{-5} \pm 8 \times 10^{-7}$	$6 \times 10^{-5} \pm 8 \times 10^{-6}$

PD1, PD2, and PD3: Probabilities of detached states D1, D2, and D3 respectively.

PA1, PA2, and PA3: Probabilities of attached states A1, A2, and A3 respectively.

– Pr \* lnPr : dimensionless elements;  $-R \sum_r (Pr * \ln Pr)$  represents the statistical entropy.

while PA3 was the lowest. Values of  $-(Pr * \ln Pr)$ , ( $r = 1$  to 6) are shown in Table 2. As molar statistical entropy ( $S$ ) is equal to  $-R * \sum_r (Pr * \ln Pr)$ , it can be seen that steps D2 and D3 made an important contribution to  $S$ , particularly in heart and TSM.

3.3. Relationships between muscle and CB parameters

There was a complex relationship between  $Po$  and  $N$  (Fig. 5A), partly because mean values of total tension and crossbridge number ( $N$ ) did not differ between heart and diaphragm (tw) ( $P = 0.007$ ) (Fig. 3A and D), although that of  $\pi$  was different ( $P < 0.001$ ) (Fig. 3C). The heart group appeared to be separate from the 3 other groups approximately arranged in a linear manner. Conversely, there was no relationship between  $Po$  and  $\pi$  (Fig. 5C). Fig. 5B shows a non linear inverse relationship between maximum efficiency and the microcanonical partition function ( $z$ ). There was a curvilinear and inverse relationship between  $G$  curvature and FDF (Fig. 5D). Normalized rate of total energy  $E_{Hux}/(Po * Vmax)$ , normalized mechanical power  $(P * V) / (Po * Vmax)$ , and efficiency as a function of  $P/Po$  are presented in Fig. 6. For  $E_{Hux}/(Po * Vmax)$  and  $(P * V) / (Po * Vmax)$ , maximum values were observed in cardiac muscle and minimum values in diaphragm (tet) (Fig. 6A and B). For efficiency, opposite results were registered (Fig. 6C).

3.4. Statistical mechanics parameters

Statistical entropy ( $S$ ) reached the highest values in heart ( $P < 0.001$  versus the other 3 groups) and the lowest value in diaphragm (tet) ( $P < 0.001$  versus the other 3 groups) (Fig. 7A). This was explained by the high values of  $(PD2 * \ln PD2)$  and  $(PD3 * \ln PD3)$  in the heart and their low

values in diaphragm (tet) (Table 2). In both diaphragm (tw) and diaphragm (tet),  $S$  was significantly lower than in heart and TSM. However,  $S$  was statistically higher in diaphragm (tw) than in diaphragm (tet) ( $P < 0.001$ ). Internal energy ( $E$ ) behaved in a fairly similar manner to  $S$ , except that  $E$  did not differ between heart and TSM ( $P = 0.060$ ) (Fig. 7B). Comparisons for the energy ( $E - TS$ ) (Fig. 7C) were similar to  $S$ . Grand potential reached the highest negative value in heart ( $P < 0.001$  versus the other 3 groups) and the lowest value in diaphragm (tet) ( $P < 0.001$  versus heart and TSM) (Fig. 7D). Grand potential did not differ between diaphragm (tw) and (tet). Grand potential was moderately, yet significantly less negative in TSM than in heart.

Affinity ( $A$ ) was significantly lower in diaphragm (tet) than in the other 3 groups ( $P < 0.03$  versus the 3 other groups) (Fig. 8C). However,  $A$  did not significantly differ between heart, trachea and diaphragm (tw). Thermodynamic force ( $A/T$ ) behaved similarly to  $A$  (Fig. 8A). Thermodynamic flow ( $v$ ) was markedly higher in heart than in the other 3 groups ( $P < 0.001$  versus the other 3 groups) (Fig. 8B). Similarly, the rate of entropy production ( $A/T * v$ ) reached the highest value of all the groups in heart ( $P < 0.001$  versus the other 3 groups) (Fig. 8D).

Fig. 9A and B show the linear relationships between thermodynamic force ( $A/T$ ) and thermodynamic flow ( $v$ ). Thus diaphragm (tet) and (tw), heart and TSM behaved in accordance with the linear stationary regime for which entropy production rate is minimal according to Prigogine's theorem [23]. Fig. 9C shows that, for a given level of affinity, statistical entropy was higher in heart and TSM than in diaphragm (tet and tw). Fig. 9D shows that the high entropy production rate observed in heart was accompanied by low CB single force, whereas the other 3 groups exhibited low entropy production rate over a large range of CB single force. Microcanonical, canonical, and grand

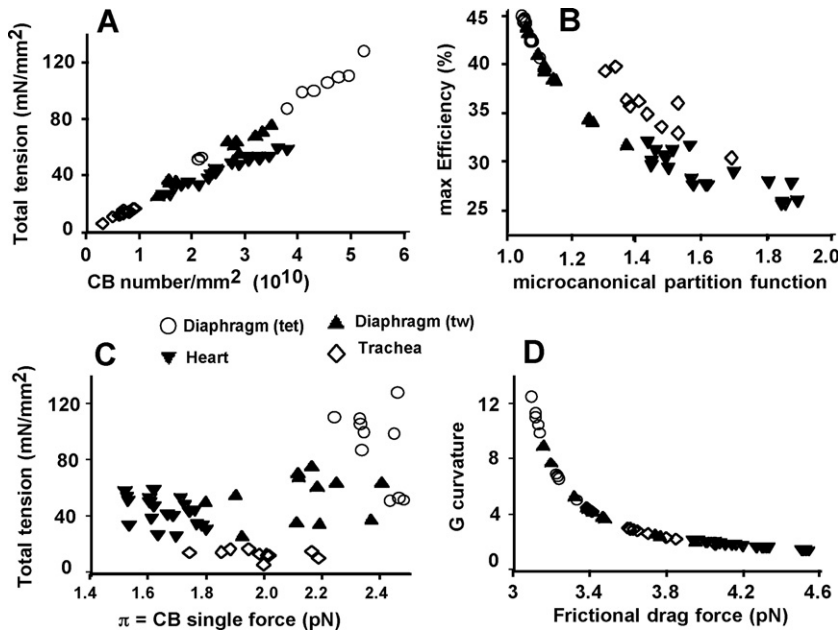


Fig. 5. Mechanical relationships. Total tension as a function of CB number/mm<sup>2</sup> (A), max Efficiency as a function of the microcanonical partition function (B), Total tension as a function of CB single force (C), G curvature as a function of frictional drag force (D).

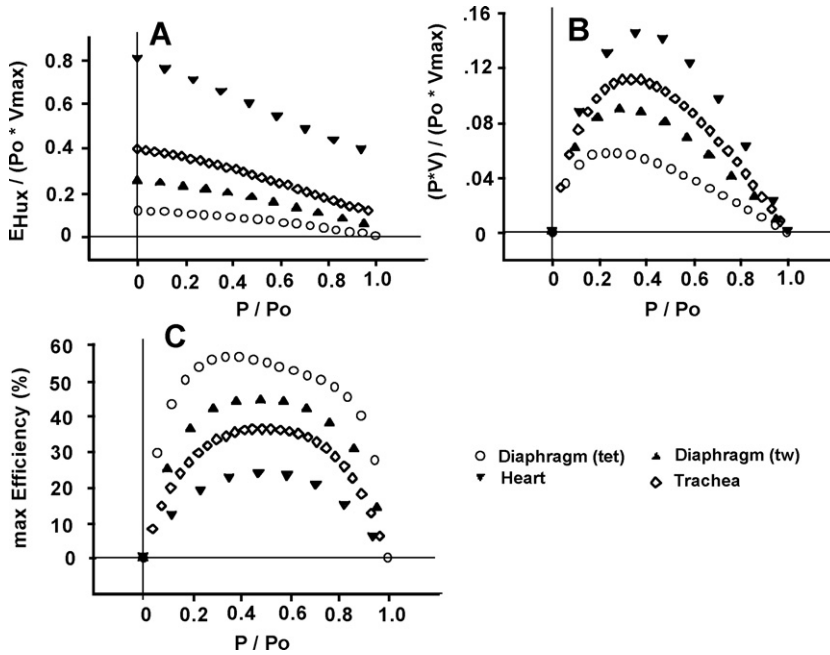


Fig. 6. Relationship between  $E_{Hux}/(P_o \cdot V_{max})$  and  $P/P_o$  (A); Relationship between  $PV/(P_o \cdot V_{max})$  and  $P/P_o$  (B); Relationship between Efficiency (%) and  $P/P_o$  (C).

canonical partition function are presented in Table 1. Statistical mechanics parameters observed in diaphragm in tetanus were close to those previously described in fast and slow skeletal muscles [7].

4. Discussion

The main purpose of this study was to compare the statistical mechanics of striated and smooth muscles. This

approach was assessed in heart, TSM and skeletal diaphragm muscle under twitch and/or tetanic conditions. Until now, such thermodynamic studies have been restricted to skeletal muscles under tetanus [7,8]. The phenomenological formalism introduced by A. Huxley makes it possible to apply statistical mechanics to striated and smooth muscles [1]. Thus, due to the huge number of CBs involved in contractile processes, a combination of both statistical mechanics [24] and A. Huxley's equations

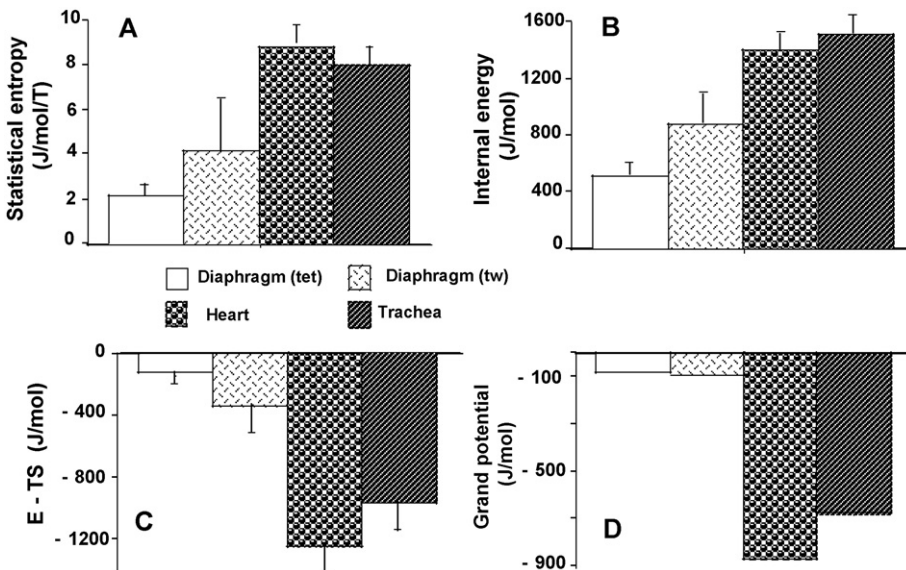


Fig. 7. Thermodynamic parameters. Statistical entropy (A). Internal energy (B). E - TS (C). Grand potential (D).

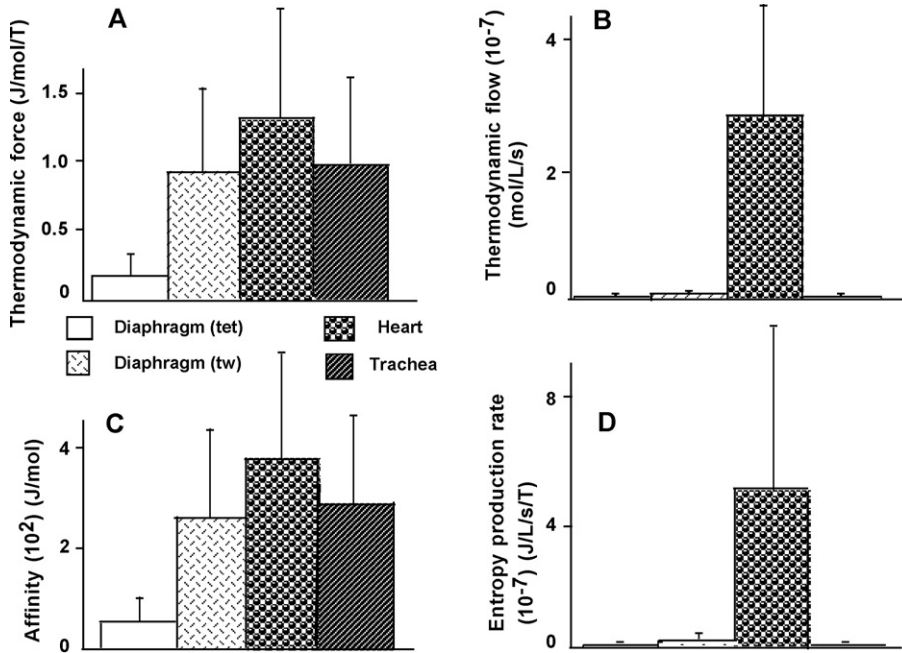


Fig. 8. Thermodynamic parameters. Thermodynamic force (A). Thermodynamic flow (B). Affinity (C). Rate of entropy production (D).

[1] can be used to determine macroscopic thermodynamic properties of living muscles [2,25].

4.1. Differences in CB kinetics between muscles

Despite considerable differences in CB attachment and detachment constants between the 4 groups studied

(Fig. 2A, B and C), CB single force ( $\pi$ ) was of the same order of magnitude even though significant differences in  $\pi$  existed between groups (Fig. 3C). However, the large range of CB kinetics encountered in the 4 groups led to a specific thermodynamic profile characterizing each of them (Figs. 7 and 8). There was a factor ranging from 1 to 20 between the highest values of  $f_1$ ,  $g_1$ , and  $g_2$

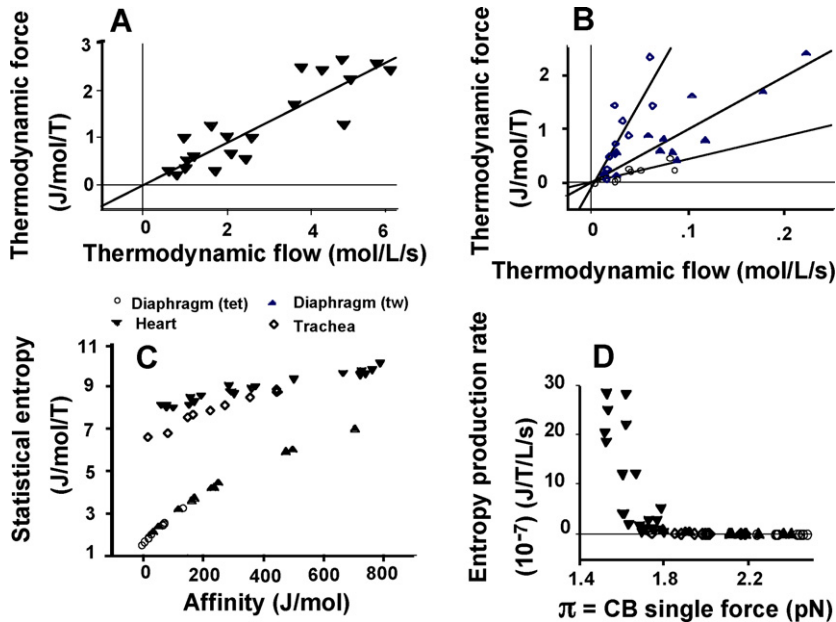


Fig. 9. Relationships between thermodynamic parameters and CB properties. Linear relationships between thermodynamic force and thermodynamic flow. Thermodynamic force = .2 Thermodynamic flow; R = .86 (Heart) (A); Thermodynamic force = 2.2 Thermodynamic flow; R = .85 (Diaphragm tet); Thermodynamic force = 5.0 Thermodynamic flow; R = .89 (Diaphragm tw); Thermodynamic force = 16.1 Thermodynamic flow; R = .82 (Trachea) (B). Statistical entropy as a function of affinity (C). Rate of entropy production as a function of CB single force (D).

observed in heart and the lowest observed in TSM (Fig. 2A, B and C).

In the heart, the high values of the attachment ( $f_1$ ) and detachment ( $g_1$  and  $g_2$ ) constants were responsible for quick attachment and detachment, and short time stroke (Fig. 2A, B and C and Fig. 4B). Moreover,  $\pi$  and Effmax were proportional to  $f_1/(f_1 + g_1)$ , although  $k_{cat}$ , and consequently the thermodynamic flow  $v$ , were proportional to  $f_1 g_1 / (f_1 + g_1)$  [26]. CB kinetics implied that in the heart, (i) CB single force was moderately but significantly lower than in the other muscles studied (Fig. 3C); (ii) maximum turnover rate of myosin ATPase ( $k_{cat}$ ), thermodynamic flow and rate of entropy production were markedly higher than in the other muscles studied (Fig. 8B and D). This may be partly explained by differences in temperature used for each muscle type but was mainly explained by high values of constants  $f_1$  and  $g_1$ . Although it has been shown that  $k_{cat}$  increases with temperature [12], the highest temperature used in our study was applied on TSM (37°C) and nevertheless this corresponded with the lowest value of  $k_{cat}$  and thermodynamic flow (Fig. 8B). The absolute value of the asymptote  $-b$  in TSM is similar to those observed in canine trachealis [27] and in other smooth muscles [28,29], and was 35-fold lower in TSM than in the heart (Table 1). The low values of  $k_{cat}$  and thermodynamic flow observed in TSM were due to low values of CB kinetics and not to temperature (Fig. 8B). Although  $Po/a$  (i.e. the curvature  $G$ ) is less temperature dependent than asymptote  $-b$ , asymptote  $-b$  is highly temperature sensitive and has a temperature coefficient of about 2.05 per 10°C [10]. By comparing with skeletal muscles, the low value of the constant  $b$  observed in smooth muscle reflects the low rate of energy expenditure [30]. Smooth muscle is capable of expending nearly as much energy as skeletal muscle, but at a slow rate. This property is reflected by a low rate of tension development and a slow velocity of shortening. Differences in statistical mechanics have been previously described in slow and fast skeletal muscles studied at same temperature and under similar stimulation conditions [7]. Thus, these differences can be partly explained by differences in the molecular structure of the myosin head. Moreover in the present study, differences in statistical mechanics were also observed in a given muscle type, i.e., diaphragm muscle, studied at same temperature but under different stimulation conditions. Thus, the stimulation mode (twitch versus tetanus) induced significant and reversible changes in statistical mechanics.

Structural, biochemical or mechanical factors may account for the large differences in CB kinetics and mechanical statistics observed between the three types of muscles studied: (i) differences in the three-dimensional structure of the myosin head either on the ATP binding pocket or on the actin-binding site [31–33]; (ii) differences in structure or function of the regulatory and essential myosin light chains, or differences in content or activity of the myosin light chain kinase (MLCK) [34]; (iii) functional differences in the calcium-calmodulin complex, etc. However, immediate changes in CB kinetics induced by switching from twitch to tetanus in diaphragm (Fig. 2A, B and C) could not be explained by alterations in the three-dimensional structure of the myosin head. It may be

hypothesized that changing the mode of electrical stimulation frequency either modifies the chemical environment of the myosin head or modulates the function of amino-acid loops localized on the ATP binding pocket or the actin-binding site of the myosin head. This could change the global activation processes of the CB molecular motors, thus determining characteristic CB attachment and detachment constants [35].

#### 4.2. Near-equilibrium thermodynamics

In the 4 groups studied, near-equilibrium thermodynamic behavior was validated because the chemical affinity (A) was  $\ll 2500 \text{ J} \cdot \text{mol}^{-1}$  (Fig. 8C) [3,23,36]. Numerous enzymatic systems in muscle cells [37,38], such as Gibbs-Donnan system in heart muscle [39], and  $\text{Na}^+ - \text{K}^+$  ATPase in all tissues [40] behave near equilibrium. Both normal and pathological skeletal muscles have been reported as behaving in a near-equilibrium state [7,8]. In the present study, the chemical affinity was significantly higher in heart, TSM, and diaphragm (tw) than in diaphragm (tet), but in all cases remained  $\ll 2500 \text{ J/mol}$  (Fig. 8C) and consequently these muscles behaved near equilibrium.

#### 4.3. Linear regime

Several biological processes behave in stationary non-equilibrium state with irreversible changes such as transport of matter and can be described by kinetic equations. Complex coupled phenomena obey phenomenological laws such as the mass action law between affinities and reaction rates, and Fick's law between a substance flow and its concentration gradient. A flow can be generated against its conjugate force through these kinds of coupling. In our study, thermodynamic force ( $A/T$ ) varied linearly with thermodynamic flow ( $v$ ), so that the system was stationary (Fig. 9A and B) [41]. In such stationary linear regime, Prigogine's theorem can be applied [23]: in the linear regime, total entropy production rate in a system subject to flow of energy and matter reaches a minimum value at the non-equilibrium stationary state. Linear near-equilibrium thermodynamics [5] have been previously reported in numerous fields of living systems, including mitochondria and oxidative phosphorylation, facilitated and active transport [42–46], and time evolution of proteins [47]. Such a linear regime has also been reported in normal skeletal muscles [7] and pathological diaphragm muscles [8].

#### 4.4. Statistical entropy

Statistical entropy ( $S$ ) is related to the dispersal of energy and represents a measure of the degree of disorder in a given system [2,48]. Statistical entropy is equal to  $-R \sum_r (\text{Pr}^* \ln \text{Pr})$ .  $S$  was markedly higher in heart and TSM than in diaphragm (tw and tet) (Fig. 7A), because the values of  $-(\text{Pr}^* \ln \text{Pr})$  were higher in heart and TSM than in diaphragm (tet) and (tw) (Table 2). In both heart and TSM, the high values of  $S$  contrasted on the one hand with the high values of  $V_{max}$  and CB kinetics constants in heart and, on the other, with the low values of  $V_{max}$  and CB kinetics

constants in TSM (Fig. 3B and Fig. 2A, B and C). The absolute value of  $(E - TS)$  mimicked the profile of  $S$  (Fig. 7A and C). Conversely, the profile of CB single force ( $\pi$ ) (Fig. 3C) appeared opposite to that of both  $S$  and the absolute value of  $(E - TS)$ .  $S$  and the molecular partition function ( $z$ ) evolved similarly (Fig. 7A and Table 1). The molecular partition function ( $z$ ) reflects how the total number of molecular motors is distributed – partitioned – over the available states. The value of  $z$  gives a rough estimate of the number of molecular states that are significantly populated at  $T^\circ\text{K}$ . Thus, it has been shown that  $S$  and  $z$  increase when both  $\text{Effmax}$  and CB single force  $\pi$  decrease [8].

#### 4.5. Entropy production

Entropy production rate quantifies irreversibility [23]. The higher the rate of entropy production, the further the system moves away from equilibrium [3]. In terms of entropy production rate, the heart played a distinctive role (Fig. 8D) due to the fact that its value was dramatically higher than in diaphragm (tet and tw) and in TSM (Fig. 8D) and in normal skeletal muscle [7] and pathological diaphragm muscle [8]. In the heart, both the high thermodynamic force ( $A/T$ ) and, to a greater extent, the high thermodynamic flow ( $v$ ) contributed to the generation of an important entropy production rate. In the present study, this highlighted the difference between statistical entropy, which is inversely related to CB single force (Fig. 3C and Fig. 7A) and muscle efficiency, and entropy production rate, which is linked to irreversible chemical processes in CB molecular motors (Fig. 8D). Although the heart and TSM exhibited comparable statistical entropy (Fig. 7A), their entropy production rate differed drastically, being high in heart and low in TSM (Fig. 8D). Differences in temperature could not account for this result because thermodynamic flow ( $v$ ) is very sensitive to temperature which was  $37^\circ\text{C}$  in TSM and  $29^\circ\text{C}$  in heart. The high value of entropy production rate observed in heart muscle indicated that this muscle generated more irreversible biochemical processes and behaved farther from equilibrium than TSM and diaphragm (tet and tw).

#### 4.6. Limitations of the study

The variables used to characterize CB kinetics and statistical mechanics were calculated but not measured. Despite the contribution made by optical tweezers [22] and X-ray crystallography [14,15], uncertainties remained concerning the exact values of the constants “ $h$ ” and “ $l$ ” in A. Huxley’s equations. These constants may differ according to either muscle type or animal species. Moreover, only one species was studied and for each muscle type, only one temperature was applied. The temperature was not  $37^\circ\text{C}$  except for TSM, but for each muscle type, the applied temperature induced the best mechanical response and stability.

#### 5. Conclusion

CB kinetics derived from A. Huxley’s equations conferred a characteristic profile in terms of statistical

mechanics on each muscle type. Statistical entropy, chemical affinity, and rate of entropy production differed in all studied muscles. Normal striated muscles (heart and diaphragm) and smooth muscle (TSM) behaved near equilibrium and in a stationary linear regime. Crossbridge kinetics and statistical mechanics, particularly the rate of entropy production partly depended on the molecular structure of the myosin molecular motor *per se*. Moreover, changes in stimulation conditions also modulated the thermodynamic variables in a reversible manner. This may be of pathophysiological importance in skeletal muscles in which the tetanic stimulation frequency may change *in vivo*, and in heart muscle which behave in twitch mode.

#### Disclosure of interest

The authors declare that they have no conflicts of interest concerning this article.

#### Acknowledgments

We thank Dr Christian Allard, “Président de la Commission médicale d’établissement de l’hôpital de Meaux”, France, Dr Michel Grivaux, “Directeur du centre de recherche clinique de l’hôpital de Meaux” and Mrs Cindy Mathis, for laboratory facilities.

#### References

- [1] A.F. Huxley, Muscle structure and theories of contraction, *Prog. Biophys. Biophys. Chem.* 7 (1957) 255–318.
- [2] P.W. Atkins, *Physical Chemistry*, Oxford University Press, Oxford/Melbourne/Tokyo, 1990.
- [3] D. Kondepudi, I. Prigogine, *Modern thermodynamics from heat engines to dissipative structures*, Wiley & Sons, New York, 1999.
- [4] R.W. Lymn, E.W. Taylor, Mechanism of adenosine triphosphate hydrolysis by actomyosin, *Biochemistry* 10 (1971) 4617–4624.
- [5] Y. Demirel, S.I. Sandler, Thermodynamics and bioenergetics, *Biophys. Chem.* 97 (2002) 87–111.
- [6] G. Nicolis, I. Prigogine, Symmetry breaking and pattern selection in far-from-equilibrium systems, *Proc. Natl Acad. Sci. U S A* 78 (1981) 659–663.
- [7] Y. Lecarpentier, F.X. Blanc, J. Quillard, J.L. Hebert, X. Krokidis, C. Coirault, Statistical mechanics of myosin molecular motors in skeletal muscles, *J. Theor. Biol.* 235 (2005) 381–392.
- [8] Y. Lecarpentier, X. Krokidis, P. Martin, T. Pineau, J.L. Hebert, J. Quillard, M. Cortes-Morichetti, C. Coirault, Increased entropy production in diaphragm muscle of PPAR alpha knockout mice, *J. Theor. Biol.* 250 (2008) 92–102.
- [9] Y. Lecarpentier, F.X. Blanc, S. Salmeron, J.C. Pourny, D. Chemla, C. Coirault, Myosin cross-bridge kinetics in airway smooth muscle: a comparative study of humans, rats, and rabbits, *Am. J. Physiol. Lung Cell Mol. Physiol.* 282 (2002) L83–L90.
- [10] A.V. Hill, The heat of shortening and the dynamic constants of muscle, *Proc. R. Soc. Lond. Biol. Sci.* 126 (1938) 136–195.
- [11] Y. Lecarpentier, D. Chemla, F.X. Blanc, J.C. Pourny, T. Joseph, B. Riou, C. Coirault, Mechanics, energetics, and crossbridge kinetics of rabbit diaphragm during congestive heart failure, *FASEB J.* 12 (1998) 981–989.
- [12] R.C. Woledge, A.N. Curtin, E. Homsher, *Energetic aspects of muscle contraction*, Academic Press, London, 1985.
- [13] A.F. Huxley, R.M. Simmons, Proposed mechanism of force generation in striated muscle, *Nature* 233 (1971) 533–538.
- [14] I. Rayment, W.R. Rypniewski, K. Schmidt-Base, R. Smith, D.R. Tomchick, M.M. Benning, D.A. Winkelmann, G. Wesenberg, H.M. Holden, Three-dimensional structure of myosin subfragment-1: a molecular motor, *Science* 261 (1993) 50–58.
- [15] R. Dominguez, Y. Freyzon, K.M. Trybus, C. Cohen, Crystal structure of a vertebrate smooth muscle myosin motor domain and its complex with the essential light chain: visualization of the pre-power stroke state, *Cell* 94 (1998) 559–571.

- [16] W.O. Fenn, A quantitative comparison between the energy liberated and the work performed by the isolated sartorius muscle of the frog, *J. Physiol. Lond.* 58 (1923) 175–203.
- [17] E. Homsher, W.F. Mommaerts, N.V. Ricciuti, Energetics of shortening muscles in twitches and tetanic contractions. II. Force-determined shortening heat, *J. Gen. Physiol.* 62 (1973) 677–692.
- [18] J.A. Rall, Sense and nonsense about the Fenn effect, *Am. J. Physiol.* 242 (1982) H1–H6.
- [19] W.F. Mommaerts, Energetics of muscular contraction, *Physiol. Rev.* 49 (1969) 427–508.
- [20] H. Suga, Energetics of the time-varying elastance model, a visco-elastic model, matches Mommaerts' unifying concept of the Fenn effect of muscle, *Jpn Heart J.* 31 (1990) 341–353.
- [21] J. Howard, Molecular motors. Clamping down on myosin, *Nature* 368 (1994) 98–99.
- [22] J.T. Finer, R.M. Simmons, J.A. Spudich, Single myosin molecule mechanics: piconewton forces and nanometre steps, *Nature* 368 (1994) 113–119.
- [23] I. Prigogine, Introduction to thermodynamics of irreversible processes, Wiley J., New York, 1967.
- [24] I.N. Levine, Physical chemistry, Mc Graw Hill, New York, 2003.
- [25] P. Backx, Efficiency of cardiac muscle: thermodynamic and statistical mechanical considerations, *Basic Res. Cardiol.* 88 (Suppl. 2) (1993) 21–28.
- [26] A. Weisberg, S. Winegrad, Relation between crossbridge structure and actomyosin ATPase activity in rat heart, *Circ. Res.* 83 (1998) 60–72.
- [27] N.L. Stephens, Force-velocity constants in smooth muscle: afterloaded isotonic and quick-release methods, *Can. J. Physiol. Pharmacol.* 63 (1985) 48–51.
- [28] A. Csapo, Dependence of isometric tension and isotonic shortening of uterine muscle on temperature and on strength of stimulation, *Am. J. Physiol.* 177 (1954) 348–354.
- [29] A.R. Gordon, M.J. Siegman, Mechanical properties of smooth muscle. I. Length-tension and force-velocity relations, *Am. J. Physiol.* 221 (1971) 1243–1249.
- [30] E. Bulbring, Measurements of oxygen consumption in smooth muscle, *J. Physiol.* 122 (1953) 111–134.
- [31] I. Rayment, H.M. Holden, M. Whittaker, C.B. Yohn, M. Lorenz, K.C. Holmes, R.A. Milligan, Structure of the actin-myosin complex and its implications for muscle contraction, *Science* 261 (1993) 58–65.
- [32] A.M. Lauzon, M.J. Tyska, A.S. Rovner, Y. Freyzo, D.M. Warshaw, K.M. Trybus, A 7-amino-acid insert in the heavy chain nucleotide binding loop alters the kinetics of smooth muscle myosin in the laser trap, *J. Muscle Res. Cell. Motil.* 19 (1998) 825–837.
- [33] S. Winegrad, How actin-myosin interactions differ with different isoforms of myosin, *Circ. Res.* 82 (1998) 1109–1110.
- [34] K.M. Trybus, Role of myosin light chains, *J. Muscle Res. Cell. Motil.* 15 (1994) 587–594.
- [35] J.A. Spudich, How molecular motors work, *Nature* 372 (1994) 515–518.
- [36] I. Prigogine, G. Nicolis, A. Babloyantz, Nonequilibrium problems in biological phenomena, *Ann. N Y Acad. Sci.* 231 (1974) 99–105.
- [37] R.L. Veech, J.W. Lawson, N.W. Cornell, H.A. Krebs, Cytosolic phosphorylation potential, *J. Biol. Chem.* 254 (1979) 6538–6547.
- [38] W.E. Marshall, A. Omachi, Measured and calculated NAD<sup>+</sup>-NADH ratios in human erythrocytes, *Biochim. Biophys. Acta* 354 (1974) 1–10.
- [39] T. Masuda, G.P. Dobson, R.L. Veech, The Gibbs-Donnan near-equilibrium system of heart, *J. Biol. Chem.* 265 (1990) 20321–20334.
- [40] R.L. Veech, Y. Kashiwaya, D.N. Gates, M.T. King, K. Clarke, The energetics of ion distribution: the origin of the resting electric potential of cells, *IUBMB Life* 54 (2002) 241–252.
- [41] L. Onsager, Reciprocal relations in irreversible processes II, *Phys. Rev.* 38 (1931) 405–426.
- [42] M. Rigoulet, A. Devin, P. Espie, B. Guerin, E. Fontaine, M.A. Piquet, V. Nogueira, X. Leverve, Flux-force relationships in intact cells: a helpful tool for understanding the mechanism of oxidative phosphorylation alterations? *Biochim. Biophys. Acta* 1365 (1998) 117–124.
- [43] J.W. Stucki, The optimal efficiency and the economic degrees of coupling of oxidative phosphorylation, *Eur. J. Biochem.* 109 (1980) 269–283.
- [44] J.W. Stucki, Non-equilibrium thermodynamic sensitivity of oxidative phosphorylation, *Proc. R. Soc. Lond. B Biol. Sci.* 244 (1991) 197–202.
- [45] O. Kedem, A. Katchalsky, Thermodynamic analysis of the permeability of biological membranes to non-electrolytes, 1958, *Biochim. Biophys. Acta* 1000 (1989) 413–430.
- [46] S.R. Caplan, A. Essig, Oxidative phosphorylation: thermodynamic criteria for the chemical and chemiosmotic hypotheses, *Proc. Natl Acad. Sci. U S A* 64 (1969) 211–218.
- [47] T.G. Dewey, M. Delle Donne, Non-equilibrium thermodynamics of molecular evolution, *J. Theor. Biol.* 193 (1998) 593–599.
- [48] I. Prigogine, G. Nicolis, Biological order, structure and instabilities, *Q. Rev. Biophys.* 4 (1971) 107–148.